Journal of the European Ceramic Society 21 (2001) 2331–2344
www.elsevier.com/locate/jeurceramsoc

Electrical properties of dense Me-doped bismuth vanadate (Me = Cu, Co) pO_2-dependent conductivity determined by impedance spectroscopy

M. Guillodo [a,*], J. Fouletier [a], L. Dessemond [a], P. Del Gallo [b]

[a] *Laboratoire d'Electrochimie et de Physicochimie des Matériaux et des Interfaces, 38402-Saint Martin d'Hères, France*
[b] *L'AIR LIQUIDE, Centre de Recherches Claude Delorme, 78354-Jouy en Josas, France*

Received 17 November 2000; received in revised form 2 February 2001; accepted 17 February 2001

Abstract

Co- and Cu-substituted $Bi_4V_2O_{11}$ compounds were synthesised by means of fine reactive powders with a typical d_{50} close to 0.5 μm. Appropriate sintering conditions resulted in fine and homogeneous microstructure without any cracks related to large grain size. The total electrical conductivity was measured by complex impedance spectroscopy with respect to temperature, oxygen partial pressure, thermal history, and nature of dopant. The bulk and the grain boundary conductivity were also studied for both compounds. No time-dependence and no thermal hysteresis of the total electrical conductivity were observed and a structure dependence of the electrical properties was noticed. BICUVOX0.10 material can be considered as a pure oxide ion conductor within the investigated experimental conditions whereas BICOVOX0.10 exhibited a p-type conductivity contribution to the bulk conductivity with an ionic transference number greater than 0.97.

Keywords: $Bi_4V_2O_{11}$; Electrical conductivity; Grain boundaries; Impedance spectroscopy; Ionic conductivity

1. Introduction

Me-substituted bismuth vanadate is generally known under the acronym BIMEVOX in the large family of solid oxide electrolytes. These compounds exhibit high ionic conductivity at fairly low temperature[1] and have become potential candidates, particularly in small-scale ceramic oxygen generators (COGs) for aeronautical or medical applications. COGs can be classified in two categories depending on the nature of the driving force for oxygen separation: pressure or electric potential gradient. In the first, the dense ceramic membrane is a mixed ionic-electronic conductor (MIEC) which has an oxygen pressure gradient applied across the membrane. The separation using an MIEC membrane is schematically shown in Fig. 1. The oxygen partial pressure gradient gives rise to a chemical potential gradient, which results in migration of oxygen ions through the membrane from the high to the low $p(O_2)$ side. The MIEC membrane must present several physical or chemical properties such as (i) an electronic transport number close to 0.5 and (ii) a high oxygen surface exchange coefficient. The electrically driven configuration is more complicated to develop in terms of ceramic process. Indeed, it requires electrodes on each side of an ionic conductor used as a membrane and an external circuit. Several criteria must be respected for electrodes such as (i) a good gas permeation, (ii) a sufficient electrical conduction and (ii) a good agreement between the thermal expansion coefficient of the electrode material and that of the dense ceramic membrane. Both cathode and anode electrodes are submitted to the electrochemical dissociation and recombination of molecular oxygen, respectively. This second concept presents the real advantage of delivering large fluxes of molecular oxygen at high pressure for temperature ranges as low as 800°C, eliminating the need for compressors.

Several distinct structural groups have been proposed as solid electrolytes, such as fluorite types,[2–4] perovskites,[5,6] intergrowth perovskites/Bi_2O_2 layers[7,8] and pyrochlore compounds.[9] Intergrowth perovskite/Bi_2O_2 layer-type-oxide conductors concern all the BIMEVOX

* Corresponding author. Tel.: +33-4-7682-6574; fax: +33-4-7682-6670.
E-mail address: mickael.guillodo@lepmi.inpg.fr (M. Guillodo).

0955-2219/01/$ - see front matter
PII: S0955-2219(01)00214-X

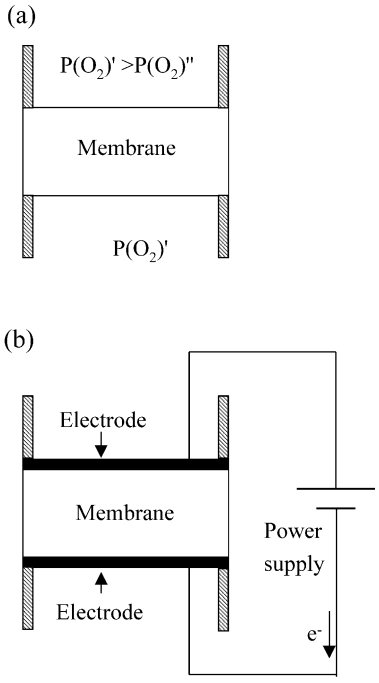

Fig. 1. Schematic representation of the two main membrane concepts for the oxygen separation according to (a) a pressure or (b) an electrical potential gradient.

compounds. These oxide-ion conductors derive from $Bi_4V_2O_{11}$ by substitution of a transition metal (Cu^{2+},[8] Co^{2+},[10] Zn^{2+},[11] Mg^{2+},[10] Ni^{2+} [12]) for vanadium in order to stabilise the γ-form of bismuth vanadate. $Bi_4Me_{0.2}V_{1.8}O_{11-x}$ (Me=Cu, Co) referred to as BIMEVOX0.10 is characterised by a γ′-form below 560°C and a γ-form beyond. Because of the layered structure, a two-dimensional oxide-ion conduction process takes place in the $(VO_3\square_{0.5})^{2-}$ layers. This strong anisotropic character was observed by conductivity measurements on single-crystals in air[13–16] and as a function of the oxygen partial pressure.[17] The applications of BIMEVOX compounds in COG require, among other things, stable and reproducible conduction properties. A strong dependence on the conductivity in their thermal history was clearly identified in the literature[12,16,18,19] by the occurrence of thermal hysteresis on the related Arrhenius diagram but there is still some controversy in the explanations.[20] As for other conducting ceramics, the electrical properties of polycrystalline BIMEVOX materials are also influenced by microstructural features, which strongly depend on the sintering procedure.[21,22] The peculiar feature is that without any significant control of both microstructure and composition, a time-dependence of the conductivity is always recorded.[13,23] This situation was recently clarified by sintering fine reactive powders (d_{50} equal to 0.50 μm) of BICOVOX0.10 at relatively low temperature, typically 750°C, for shorter times, typically 1 h.[24] Because of a fine homogeneous microstructure the formation and growth of cracks was thus avoided and neither thermal hysteresis nor time evolution of the electrical conductivity were observed. This result was confirmed in this study for cobalt- and copper-doped bismuth vanadate.

The intra- and intergranular electrical properties of dense BIMEVOX0.10 materials were investigated by impedance spectroscopy because it is a powerful technique to separate accurately both impedance contributions in polycrystalline conducting ceramics.[25–29] The results were interpreted in terms of an equivalent circuit whose parameters were determined as functions of temperature and oxygen partial pressure. This approach was also used to determine the electrolytic domain of these materials.

2. Experimental procedure

2.1. Synthesis of dense Cu- and Co-substituted $Bi_4V_2O_{11}$ materials

The BIMEVOX0.10 powder used in this study was purchased from Air Liquide (Research Center Claude Delorme, Jouy-en Josas, France). The purity of the starting powders was better than 99% and the grain size distribution was characterised by a d_{50} of about 6–8 μm. BICUVOX0.10 and BICOVOX0.10 powders were then milled by an attrition route using zirconia balls for three hours in a solvent based on ethanol. Afterwards each mixture was dried at 60°C until the weight became constant. The agglomerated powder was then sifted with a 100 μm-size sieve in order to obtain fine powders. The grain size distribution of the as-prepared powders was determined with a laser granulometer (1064, CILAS). Cylindrical green pellets were obtained by classical isostatic pressing route (typically 200 MPa for 5 min) without any additive. According to dilatometric curves recorded in air up to 800°C (heating rate: 2°C min^{-1}) using an Adamel Lhomargy (DI24) dilatometer, green bodies were sintered at 750°C for 1 h (heating rate: 3°C min^{-1}). The geometrical factors of sintered BICUVOX0.10 and BICOVOX0.10 ceramics were respectively 0.76 and 0.95 cm^{-1} and were used to normalise experimental impedance diagrams. Green and sintered densities were determined from the weight and geometric dimensions of the pellets. Hg-intrusion porosimetry (P140/P240 porosimeter, Thermoquest, France) was also performed for the sake of comparison. Both densities are referred to herein as a percentage of the theoretical ones. The crystallographic structure of BIMEVOX0.10 materials was determined by room-temperature X-ray diffraction (XRD) patterns with a Rigaku $\theta/2\theta$ diffractometer using the Bragg-Brentano geometry (0.03° in 2θ step, 1 s as a counting time) equipped with a rear monochromator (Cu $K_{\alpha 1}$ radiation, $\lambda = 1.5406$ Å). Phase composition was obtained using the Diffrac-At software

(Socabim, Paris). Particle morphologies of powders and dense membranes were characterized by means of scanning electron microscopy (SEM) (LEO S440) equipped with an energy dispersive spectrometer (EDS). The grain sizes of both sintered materials were determined according to the linear intercept method.[30]

2.2. Conductivity measurements versus oxygen partial pressure

IS measurements were performed in the 100–650°C temperature range by using an HP4192 LF impedance analyzer (Hewlett Packard) at open-circuit voltage between 5 Hz and 13×10^6 Hz with a 100 mV alternative signal. The electrochemical cell used is schematically depicted in Fig. 2. The oxygen partial pressure was monitored in the $10^{-7}-1$ bar range by means of an electrochemical oxygen pump and oxygen gauges (referred to as OG1 and OG2), upstream and downstream the electrochemical cell respectively. Variation of the order of 1% in oxygen content could be measured for any oxygen content greater than a few ppm. Both sides of BICUVOX0.10 and BICOVOX0.10 dense pellets were sputtered with a dense gold thin-film (RF sputtering, Plassys). According to S.E.M., the deposits appeared to be free from pores. Both pellets were characterised simultaneously. The rig was first heated at 100°C in an argon atmosphere (Argon U, L'Air Liquide, France) for 12 h, so that the samples were in equilibrium with the gas. Measurements were performed only when equilibrium condition was reached, i.e. after verifying that the voltages indicated by OG1 and OG2 were stable within ±1 mV over several hours. For a constant oxygen partial pressure, impedance measurements were carried out during heating and cooling cycles. This procedure was applied for several oxygen partial pressures. The isothermal dwell at any measuring temperature was typically of the three hours after temperature equilibrium condition was reached, i.e. after checking that two subsequent impedance spectra were stable over a few hours. Validation of impedance data was carried out using the Kramers–Kronig transforms.[31] This mathematical tool allowed one to check if the conditions of linearity, stability and causality of impedance spectra were obeyed at least during the measurements. Impedance spectra were represented in the commonly used Nyquist plane and data were analysed by the commercial Zview software (Version 2.1, Scribner Associates, Inc.). Equivalent circuits used by the Zview program are typically composed of resistors, R, inductances, L, capacitances, C and constant phase elements, CPE. A CPE is characterised by two parameters. The admittance, $Y(\omega)$, of a CPE can be defined as follows:

$$Y(\omega) = B.(\mathrm{j}.\omega)^n \quad (1)$$

The coefficient B and the fractional exponent n ($-1<n<1$) are the two specific parameters of a CPE. Depending on the n value, a CPE can represent discrete electrical elements. If $n=0.5$, it represents the Warburg element, used classically for modelling a semi-infinite linear diffusion. The validity of the fitting procedure was estimated according to the following methods: the χ-squared and the Weighted Sum of Squares, referred to as χ^2 and WSS, respectively.[32] The χ^2 test is the square of the deviation between the experimental and those calculated. The WSS procedure is an alternative estimation of the fitting procedure when an impedance spectrum covers a wide range of impedance. The WSS is proportional to the average percentage error between the experimental data and the calculated values. It is based on the choice of the weighting type affected to each data point.[32] We chose a calc-proportional weighting type, i.e. each data point was normalised by its magnitude.

In conventional polycrystalline ionic conductors, the impedance diagram is typically composed of a high frequency bulk semicircle (referred to as $_b$) which describes the electrical properties of the grains of the materials and a low frequency additional contribution (referred to as $_{gb}$) which represents the blocking effects of charge carriers at regular grain boundaries.[29,33,34,42] Both contributions are characterised by a resistance R_i ($i \equiv$ b or gb), a capacitance C_i ($i \equiv$ b or gb), a relaxation frequency $f_{\max,i}$ ($i \equiv$ b or gb) and a depression angle β_i ($i \equiv$ b or gb) (Fig. 3). The total resistance, R_t, and the blocking factor, α_{gb}, which is associated to the blocking effect are defined as follows:

$$R_t = R_b + R_{gb} \quad (2)$$

$$\alpha_{gb} = R_{gb}/R_t \quad (3)$$

Both semicircles of the electrolyte impedance were simulated by using R, C, L and CPE elements. The calculated values were then related to the characteristic bulk and grain boundary parameters according to the following relations:

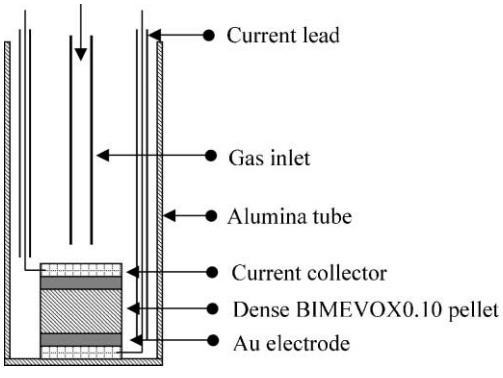

Fig. 2. Test geometry used for the electrochemical measurements.

$$f_{\max,i} = 1/\left(2.\pi.[R_i.B_i]^{1/ni}\right) \quad (4)$$

$$C_i = 1/\left(2.\pi.R_i.\ f_{\max,i}\right) \quad (5)$$

$$\beta_i = (1 - n_i).\pi/2 \quad (6)$$

3. Results and discussion

3.1. Physicochemical characterisations of BIMEVOX0.10

After ball milling by attrition, a monomodal distribution with a d_{50} equal to 0.5 μm was obtained for both powders. The XRD patterns of fine Cu- and Co-doped shown in Fig. 4 are in good agreement with those obtained by Reiselhuber et al.[22] The analysis confirmed that all the investigated powders were single phased and that no traces of second phase such as $BiVO_4$ were detected. The homogeneous chemical composition of starting powders was confirmed by EDS analysis. Below 650°C, the shrinkage behaviour of compacted BIMEVOX0.10 are nearly similar (Fig. 5). At 750°C, the linear shrinkage was equal to 14.1 and 12.3% for, respectively, BICUVOX0.10 and BICOVOX0.10. After sintering at 750°C for 1 h in air, the relative densities were at least equal to 95% of the theoretical ones (Table 1). For example, 97.3% was reached for BICUVOX0.10 according to porosimetry measurements. These results confirm that fine grain powders are required to densify BIMEVOX0.10 compounds. SEM micrographies of polished surfaces of dense BICUVOX0.10 and BICOVOX0.10 reveal that the microstructures are homogeneous in porosity and grain size distribution (Fig. 6). The mean grain sizes are, respectively, 3.3 and 2.9 μm for Cu- and Co-doped ceramics. A striking observation is that neither abnormal grain growth (in agreement with results of Fig. 5) nor intragranular cracks were detected for the chosen sintering conditions. This is in concordance with the results of Steil et al.[24] on BICOVOX0.10 and further suggests that there exists an upper grain size value to prevent any microstructural evolution during the sintering process of BIMEVOX0.10 materials. The location of pores is mainly within the grains and the density of pores on the grain boundary is neglectible as shown in Fig. 6a and b. The grain boundary is not curved for both materials (Fig. 6a and b) and one can assume that the grain growth has completely stopped.

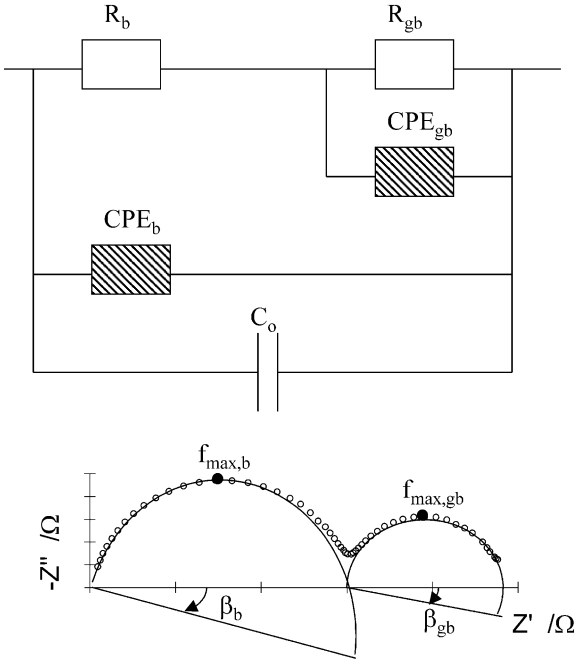

Fig. 3. Equivalent circuit used for simulation of impedance spectra of dense BICUVOX0.10 and BICOVOX0.10 in the 100–650°C temperature range and the 10^{-7}–1 bar oxygen partial pressure domain.

3.2. Equivalent circuit

The microstructure defects of the started BIMEVOX0.10 samples (i.e. regular grain boundaries) were well defined and the pore density is small. Accordingly, it was relevant to expect that the electrolyte impedance would only be composed of the high frequency bulk semicircle and the low frequency blocking effect of grain boundaries (Fig. 3). As mentioned above, the validity of electrical measurements (and thus of related variations) strongly depends on the reproducibility of conductivity values. Therefore, impedance measurements were performed during isothermal dwells and no variation of any resistive contribution was detected up to 200 h in air, as shown in Fig. 7. This result proves without any ambiguity that low grain size materials are needed for an accurate determination of the electrical properties of BIMEVOX0.10 compounds. Impedance spectra were analyzed in terms of a series association of parallel circuits and the fitting procedure of the experimental data was carried out using the equivalent circuit as shown in Fig. 3, which is based on the brick-layer model.[35–37] It is worth mentioning that the purpose of this study was not to valid any electrical model (series or parallel), but only to determine the specific parameters of each contribution (let us specify that both kinds of approach can be performed by using the impedance representation which is commonly used in the literature). The left part of the equivalent circuit is related to the bulk properties and the right part describes the additional grain boundary blocking effect. Both semicircles are characterised by a resistance and a frequency dependent dielectric dispersion. C_o represents the geometrical capacitance of the electrolyte cell and is related to the dielectric constant of the material. When the relaxation frequencies of both semicircles are sufficiently different, the electrolyte

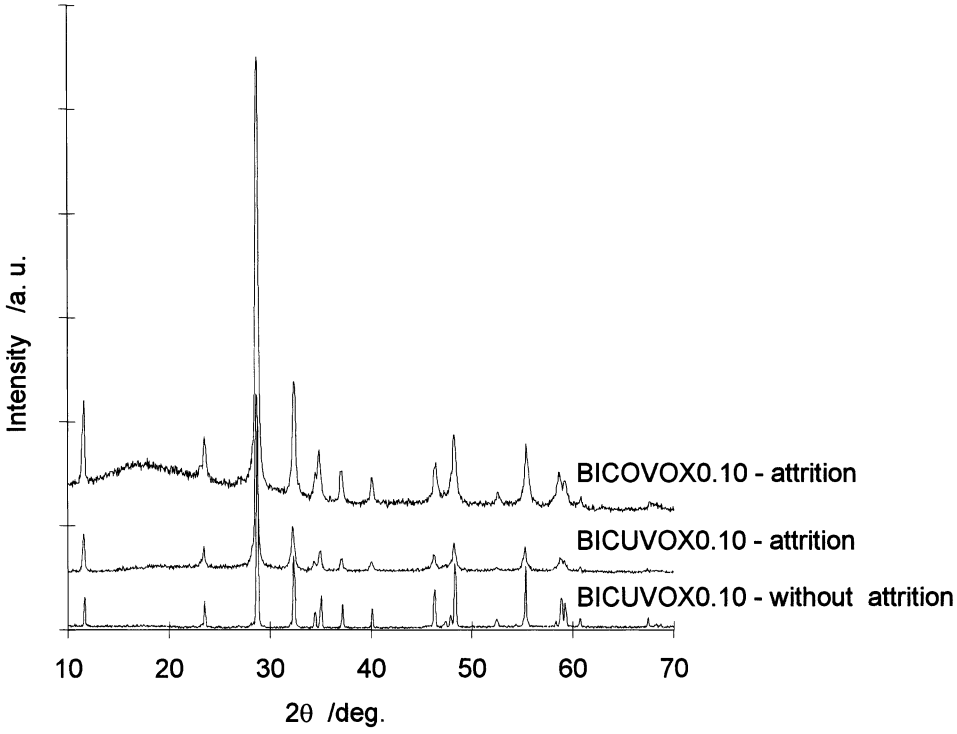

Fig. 4. XRD patterns of the two investigated BIMEVOX0.10 powders obtained after ball-milling by attrition and XRD analysis of BICUVOX0.10 without attrition ball-milling.

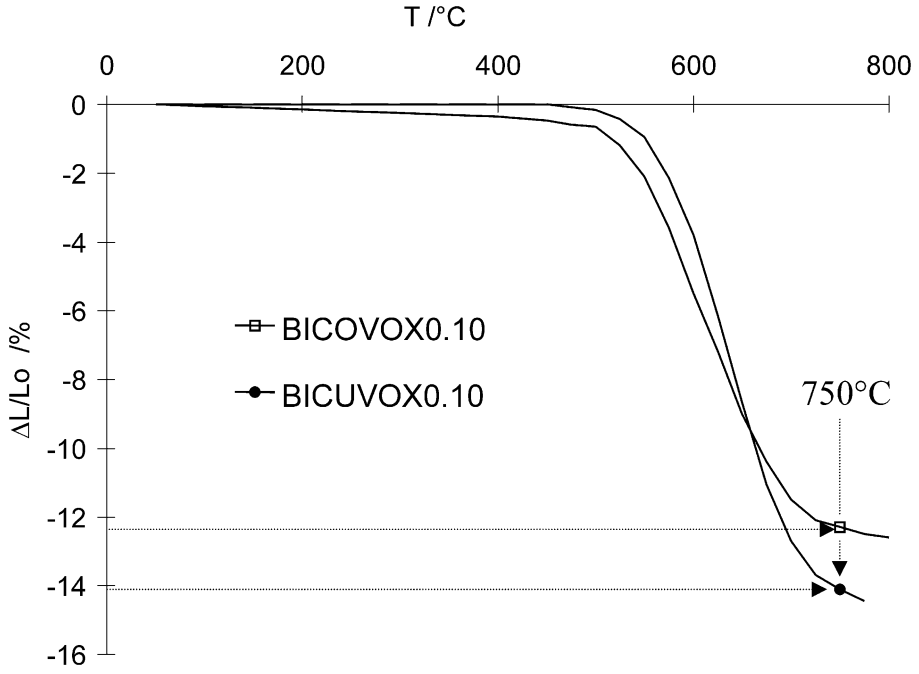

Fig. 5. Dilatometric analysis in air of green Cu- and Co-doped materials in the 20–800°C temperature range. Heating and cooling rates were 2°C min^{-1} with a holding time of 0.5 h.

impedance exhibits no overlapping (without any second phase).[38] The variations of the specific parameters were determined as functions of temperature and oxygen partial pressure. Typical electrolyte impedance diagrams recorded on Co- and Cu- doped materials are shown in Fig. 8a and b. For sake of clarity, the electrode characteristics have been subtracted. By increasing the temperature, lower impedance modulus are determined as

could be expected for thermal activated conduction processes. Impedance data can be seriously affected by residual inductance effects due to the cabling and sample holder. Moreover, the experimental frequency range is not wide enough to describe the entire diagram. In the conditions of Fig. 8a and b, the inductive tail is increasingly important at frequencies typically above 10^6 Hz. However, spectra were corrected by using a self inductance correction of about 10^{-6} H at 249°C. Whatever the measuring temperature, impedance spectra (corrected or not depending on the temperature value) were analysed in terms of the equivalent circuit of Fig. 3. The values of the specific parameters of both contributions (determined in the conditions of Fig. 8a and b) are summarised in Table 2. The low χ^2 and WSS values can be regarded as indicative of a weak standard deviation between experimental data and calculated ones. So, the chosen fitting procedure is likely to characterise the electrical parameters of BIMEVOX0.10 materials as a function of temperature in air and was extended to the variations versus oxygen partial pressure. It is worth mentioning that the additional resistance R_{gb} was regarded as no longer significant above 350°C and could not be fitted accurately. Hence, the related parameters were fixed to nil in the fitting procedure. The complete fading of the blocking effect was still described in the literature[43] and is related to an increase of the bulk conductivity of the ceramic pellet.

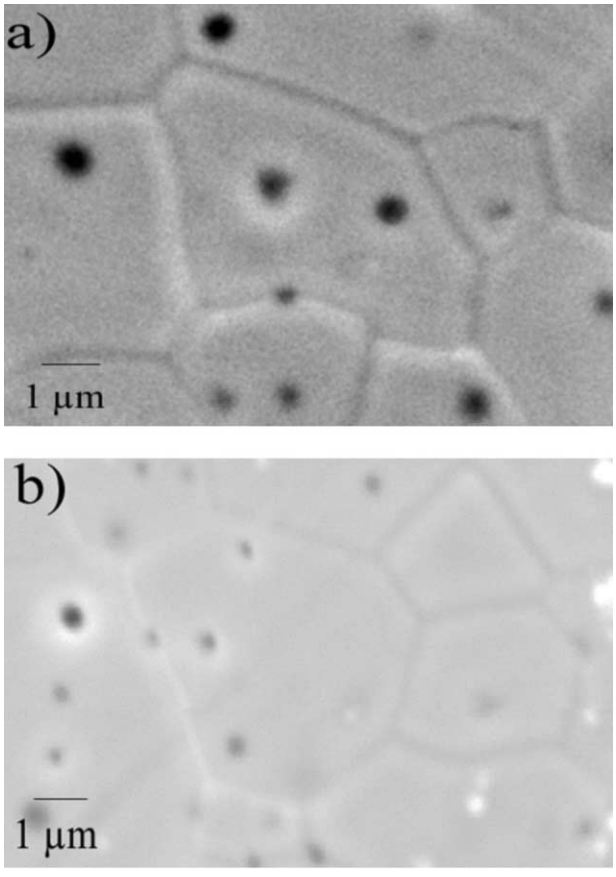

Fig. 6. SEM photograph of the microstructure of dense (a) BICUVOX0.10 and (b) BICOVOX0.10 sintered at 750°C for 1 h.

Table 1
Relative densities measured by Hg-intrusion porosimetry and geometrical dimensions of both Cu- and Co-doped materials

Material	Relative density (Hg-intrusion) (%)	Relative density (geom. dimensions) (%)
BICOVOX0.10	98	96.3
BICUVOX0.10	97.3	95

3.3. Influence of temperature in air

The first striking result is that no thermal hysteresis was evidenced within the investigated temperature range, in contradiction with previously published data.

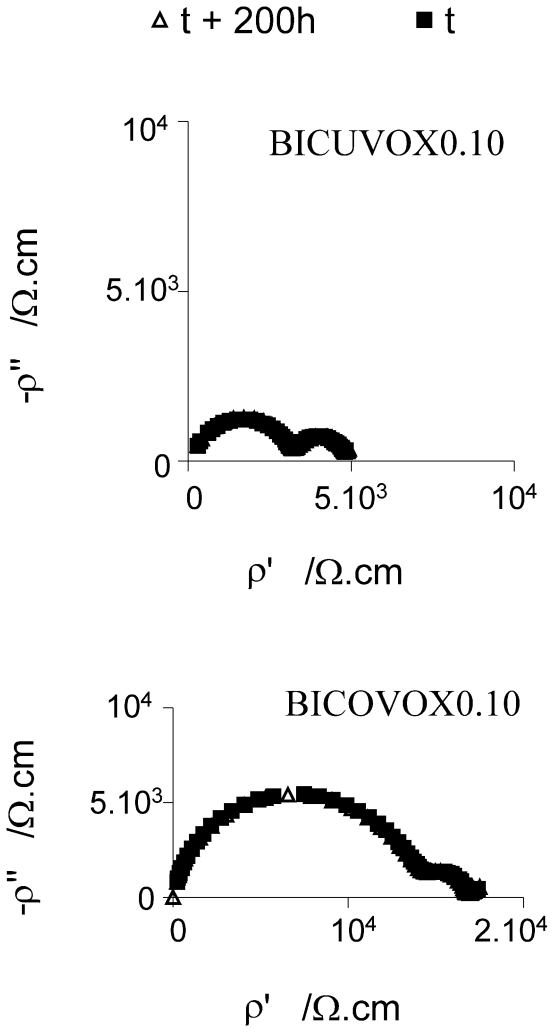

Fig. 7. Time-dependence of impedance spectra of both BICUVOX0.10 and BICOVOX0.10 measured at 190°C in air atmosphere in a time period of 200 h.

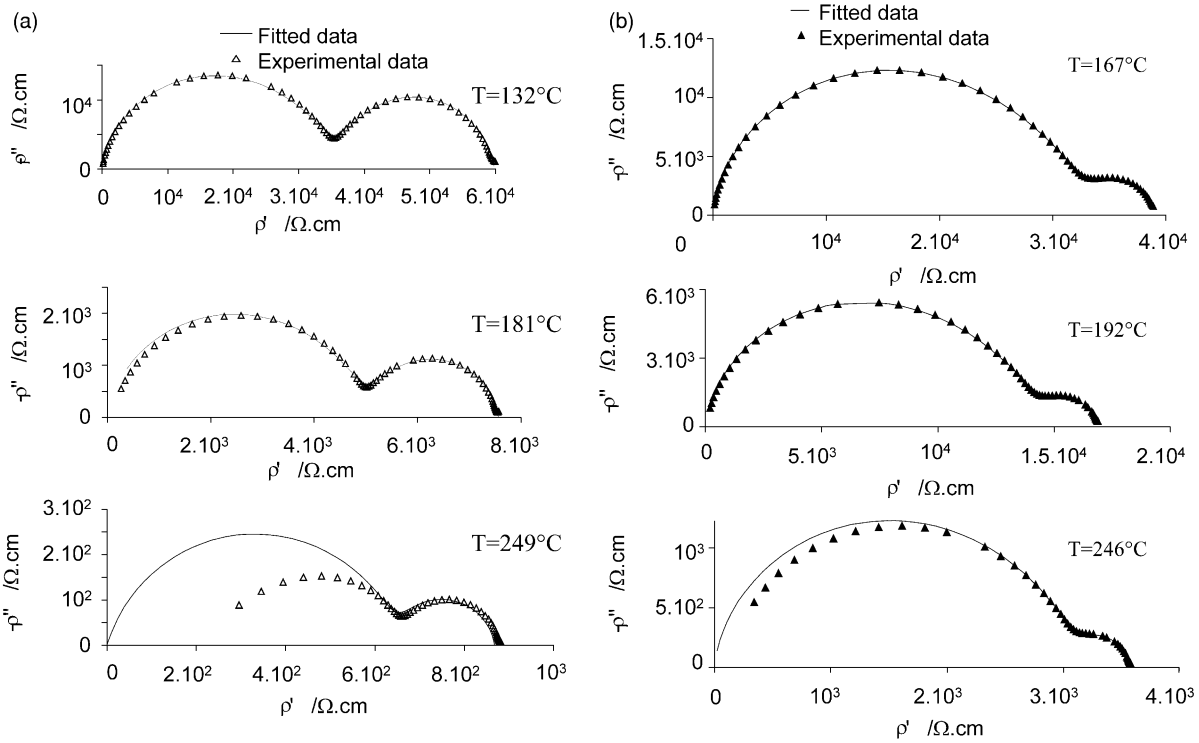

Fig. 8. Temperature dependence of fitted and experimental impedance data measured in air atmosphere for a dense (a) BICUVOX0.10 and (b) BICOVOX0.10 .

Table 2
Values of circuit parameters determined by the ZView program according to the electrical model presented in Fig. 7 of BICUVOX0.10 and BICOVOX0.10 versus three temperatures in air atmosphere[a]

	$T=132°C$		$T=181°C$		$T=249°C$	
	BICUVOX0.10	BICOVOX0.10	BICUVOX0.10	BICOVOX0.10	BICUVOX0.10	BICOVOX0.10
R_b (Ω)	28 416	170 590	3949	26 123	503.8	3060
B_b	3.42×10^{-9}	1.69×10^{-9}	2.46×10^{-9}	5.71×10^{-9}	7.18×10^{-10}	3.48×10^{-9}
n_b	0.612	0.591	0.678	0.562	0.81	0.64
R_{gb} (Ω)	17 229	22 637	1816	2526	157.6	342.1
B_{gb}	3.10×10^{-8}	8.26×10^{-8}	3.65×10^{-8}	3.43×10^{-8}	4.51×10^{-8}	2.68×10^{-8}
n_{gb}	0.909	0.769	0.915	0.947	0.914	0.96
C_o (F)	1.27×10^{-11}	8.68×10^{-12}	1.23×10^{-11}	9.04×10^{-12}	7.75×10^{-12}	9.96×10^{-12}
χ^2	1.2×10^{-3}	7.6×10^{-4}	1.5×10^{-3}	7.6×10^{-4}	1.1×10^{-3}	2.3×10^{-3}
WSS	0.148	0.087	0.160	0.074	0.083	0.194

[a] Values of χ^2 and the weighted sum of squares (WSS) are also mentioned.

Secondly, the electrolyte conductivity of BICUVOX0.10 is the highest in air whatever the measuring temperature (Fig. 9a). It mainly comes from a higher bulk conductivity. For example, σ_b is approximately 6 times that of BICOVOX0.10. This result further evidences the role of the dopant on the specific electrical properties of BIMEVOX0.10 materials. In BICOVOX0.10, the magnitude of the additional blocking resistance, R_{gb}, is larger, as generally observed in low conductivity materials.[39] Typically, a 2-fold increase was recorded within the investigated temperature range. As could be expected, all the resistive contributions are thermally activated. Hence, corresponding activation energies were determined in the Arrhenius plots. The values are summarised in Table III for both materials. In agreement with previous reports[12,40,41] a curvature was observed in air between 450 and 550°C on the Arrhenius diagrams of the electrolyte conductivity (Fig. 9a and b). This corresponds to a decrease in the activation energy from typically 0.6 eV down to 0.4 eV. The experimental values are of the order of those generally recorded for anionic conductors. This is attributed to the γ–γ' transformation.[8] In the low temperature range, the activation energy of the bulk conductivity does not depend on the nature of

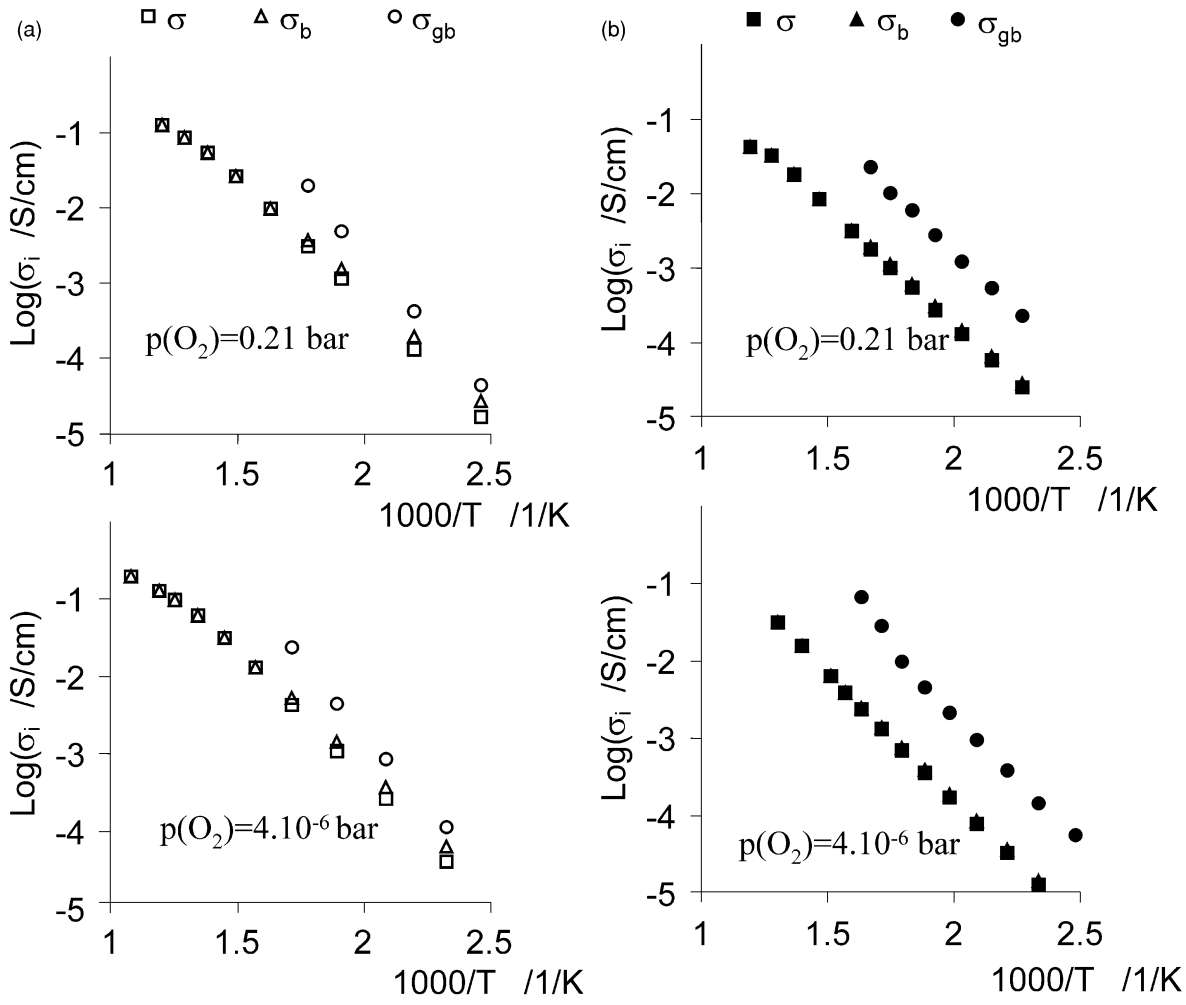

Fig. 9. (a) Arrhenius plots of electrical data (total, bulk and grain boundary conductivities) measured with a dense (a) BICUVOX0.10 and (b) BICOVOX0.10 for two oxygen partial pressures; 0.21 bar and 4×10^{-6} bar.

Table 3
Values of the activation energies E_a, $E_{a,b}$, $E_{a,gb}$ and some values of the conductivities σ, σ_b and σ_{gb} determined at 227°C (LT domain) and 627°C (HT domain) of BICUVOX0.10 and BICOVOX0.10 for the two oxygen partial pressures investigated, 0.21 bar and 4×10^{-6} bar

LT domain (below 450°C)						HT domain		
$p(O_2)$ (bar)	E_a (eV)	$E_{a,b}$ (eV)	$E_{a,gb}$ (eV)	σ (S cm^{-1}) at 227°C	σ_b (S cm^{-1}) at 227°C	σ_{gb} (S cm^{-1}) at 227°C	E_a (eV)	σ (S cm^{-1}) at 627°C
BICUVOX0.10								
0.21	0.65	0.61	0.76	6×10^{-4}	7.75×10^{-4}	2.6×10^{-3}	0.41	20×10^{-2}
4×10^{-6}	0.66	0.62	0.74	5×10^{-4}	6.6×10^{-4}	1.97×10^{-3}	0.41	18.9×10^{-2}
BICOVOX0.10								
0.21	0.62	0.61	0.65	1.4×10^{-4}	1.5×10^{-4}	1.35×10^{-3}	0.42	5.4×10^{-2}
4×10^{-6}	0.64	0.63	0.71	1.15×10^{-4}	1.23×10^{-4}	1.65×10^{-3}	0.43	5.38×10^{-2}

the dopant. A slight increase of the activation energy for the blocking conductivity was determined in agreement with literature data.[13] This is a common feature of anionic conductors in the intermediate temperature range. However, one can assume that the same conduction process occurred within both materials and that the related microstructure defects behave similarly in terms of electrical properties. The large variation in σ_b is likely to be due to an evolution of the number of available charge carriers as a function of the dopant. Fig. 10 shows the

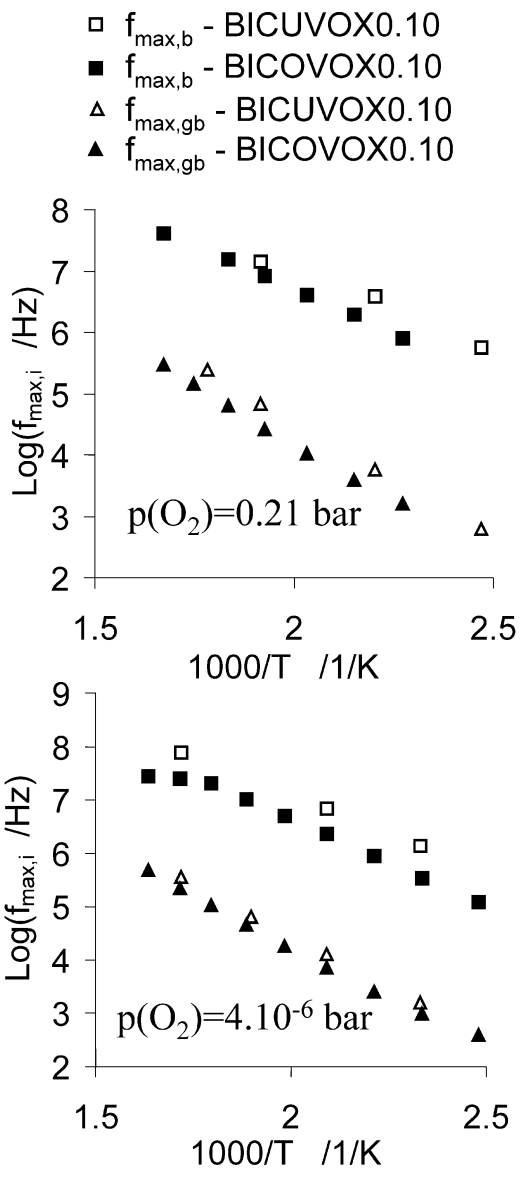

Fig. 10. Arrhenius plot of the bulk and the grain boundary relaxation frequencies measured with BICUVOX0.10 and BICOVOX0.10 materials for two oxygen partial pressures; 0.21 and 4×10^{-6} bar.

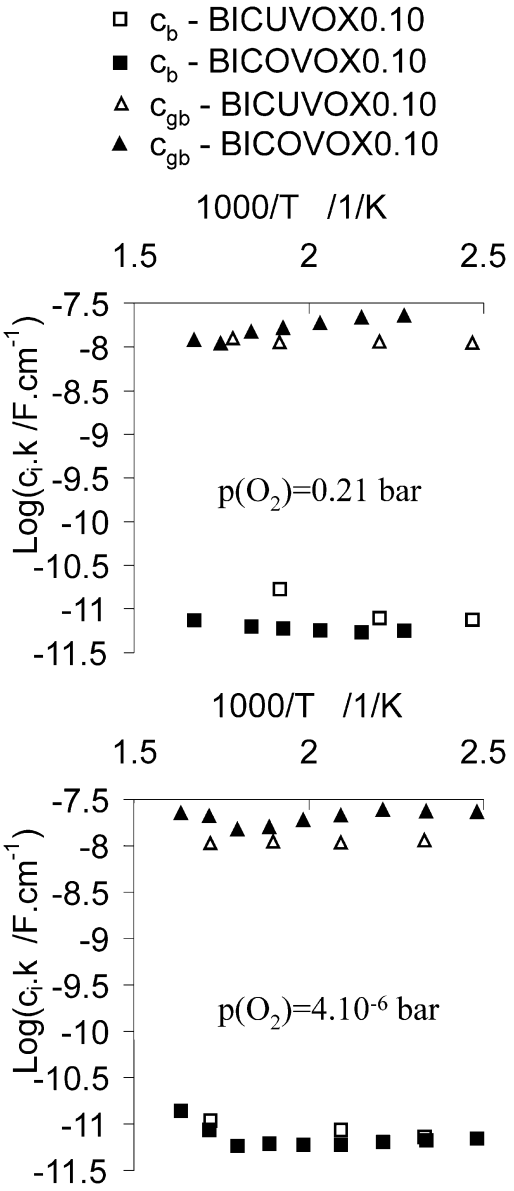

Fig. 11. Arrhenius plot of the bulk and the grain boundary capacitance measured with BICUVOX0.10 and BICOVOX0.10 materials for two oxygen partial pressures; 0.21 and 4×10^{-6} bar.

Arrhenius diagrams of the apex frequencies of both recorded semicircles (determined at the top of each contribution). In air, the bulk relaxation frequencies of both materials are close and vary in the same way as a function of temperature. The corresponding activation energy is 0.50 and 0.56 eV for BICUVOX0.10 and BICOVOX0.10 respectively. These values are in agreement with those determined for the bulk conductivity (Table 3). This indicates that the dielectric constant of both materials remained nearly identical within the measuring temperature range (Fig. 11). At 25°C, the dielectric constant is equal to 46 and 20 for Co and Cu-doped materials respectively. Accordingly, the higher values of $f_{max,b}$ for the BICUVOX0.10 material mainly comes from its higher bulk conductivity (Fig. 9a and b). For a given bulk conductivity, the relaxation frequency of a peculiar microstructure defect contribution should be nearly constant whatever its volume density[34] by assuming a low spread of related geometrical parameters. In agreement with the previous result, the apex frequency of the blocking effect of BICUVOX0.10 is slightly higher (Fig. 10). The nature of the dopant has no real influence on the value of activation energy (equal to 0.74 eV in both cases). Despite these different values, the ratio of the bulk relaxation frequency to that of the blocking effect can be regarded as nearly constant within the investigated temperature range indicating that no microstructural modification of the material occurred, in agreement with the dilatometric curves (Fig. 5). Moreover, this ratio is very similar for both materials.

All these results indicate that the average thickness of the related microstructure defects is almost identical in both materials.[43] This is further confirmed by the constancy of the blocked capacitance C_{gb} (Fig. 11). As a function of temperature, the depression angle of the blocking semicircle is nearly constant and quite low (Fig. 12). It is typically lower than 10°, in agreement with data on porous YSZ compacts.[38] This demonstrates a high homogeneity of the blocking characteristics and a narrow distribution of average geometrical parameters. Accordingly, the blocking effect is related to regular grain boundaries in both BIMEVOX0.10 materials. Let us mention that the possible influence of porosity is also included in this contribution. The bulk depression angle is fairly high whatever the measuring temperature and it drastically decreased by increasing temperature. The values are fairly close to those determined by Dygas et al.[23] The large values of β_b (Fig. 12) can be regarded as indicative of a low homogeneity of the electrical properties of the grains. However, their composition was considered as homogeneous within the samples and, so, the influence of their purity was not likely to be significant.[44] The most common interpretation of depression angle invokes a distribution of relaxation times. The high bulk depression angles could be also associated to a frequency-dependent bulk conductivity as reported by Funke et al.[45] In other words, a high depression angle can be viewed as resulting from the strong overlapping of two (or more) semicircles of very close relaxation frequencies. As already mentioned in the introduction, a strong anisotropic character of the bulk conductivity was observed for BIMEVOX single crystals in air. Despite the curvature on the Arrhenius diagram, the corresponding activation energies are nearly identical in the intermediate temperature range indicating that the electrical properties are not different regardless of the crystallographic direction.[16,17] At this stage, the high bulk depression angles of BIMEVOX0.10 materials are related to the random orientation of grains in sintered pellets resulting in a somewhat longer conduction path, as was suggested for β-aluminas.[46] Another argument in favour of this assumption is that the bulk depression angle decreases, as both conductivities become closer.

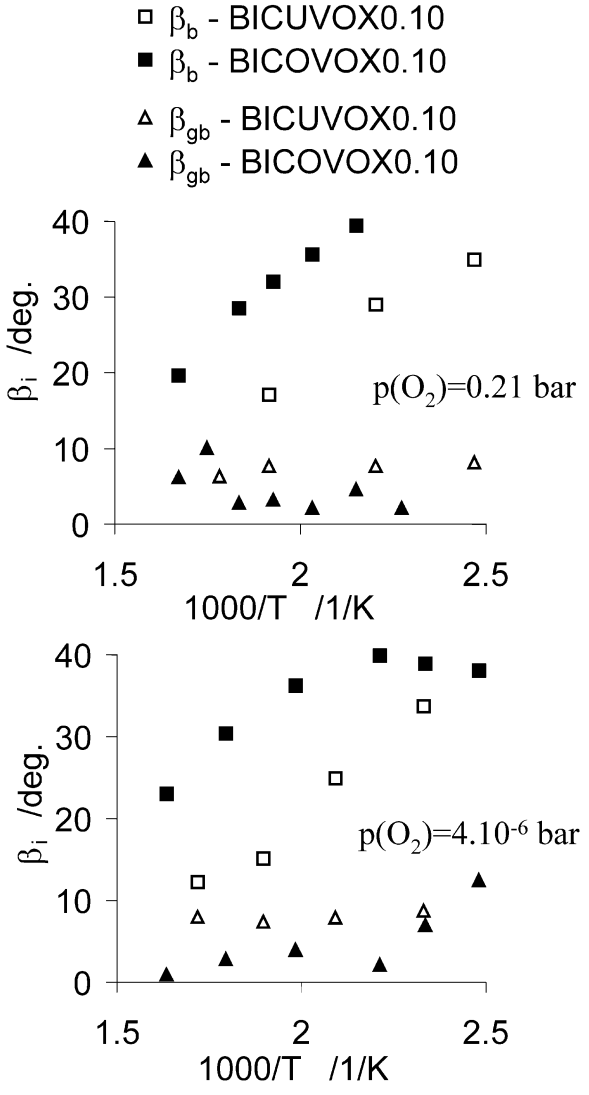

Fig. 12. Arrhenius plot of the bulk and the grain boundary depression angle measured with BICUVOX0.10 and BICOVOX0.10 materials for two oxygen partial pressures; 0.21 and 4×10^{-6} bar.

Surprising is the increase in the blocking effect in BICUVOX0.10. For temperatures below 250°C, the blocking factor [see Eq. (3)], α_{gb}, which represents the fraction of charge carriers being blocked at the corresponding microstructure defects is typically three times higher (Fig. 13). For such kinds of materials, Kim et al.[16] reported a blocking magnitude of the order of 0.2. This is not in contradiction with the lower bulk conductivity compared to the blocked one.[47] However, an increasing bulk conductivity is expected to result in a lower blocking effect, as observed experimentally[48] and as theoretically demonstrated.[39] Hence, the larger blocking effect in BICUVOX0.10 might be interpreted in terms of a lower density of intimate contacts between adjacent grains. For a given bulk conductivity, even a slight decrease in the porosity (from 3 down to 1.5%) in dense yttria-stabilised zirconia results in a large variation of the magnitude of the blocking effect.[38] Accordingly, because of a higher bulk conductivity (Fig. 9a) and a slightly higher relative density, the recorded blocking effect in BICUVOX0.10 sample might be smaller. This assumption is in perfect contradiction with the experimental results (Fig. 8a). According to Guo,[49] another explanation of the electrical grain boundary behaviour of high purity polycrystalline ceramics (without any second phase) is the formation of space-charge layers in the vicinity of grain boundaries. The nature of a space-charge layer depends on the charge of the dopant and of the level of impurities.[50–53] In both investigated materials, the substitution of vanadium by a divalent element (Co or Cu) results in solutes with the same negative

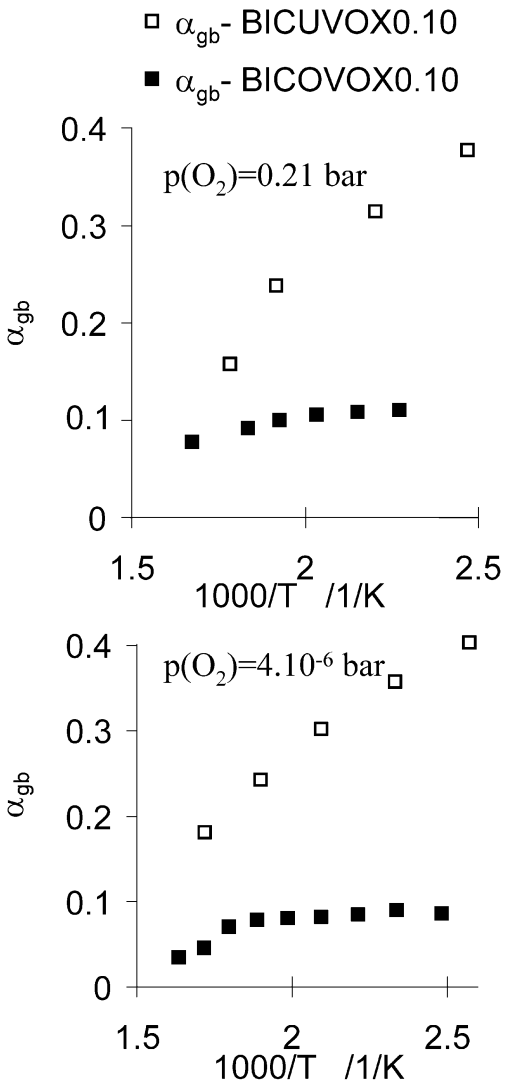

Fig. 13. Arrhenius plot of the blocking factor measured with BICUVOX0.10 and BICOVOX0.10 materials for two oxygen partial pressures; 0.21 and 4×10^{-6} bar.

effective charge, according to the Kröger–Vink notation. By assuming solute segregation to grain boundaries, the space-charge potential in BIMEVOX0.10 compounds is expected to be negative, which corresponds to an oxygen vacancies depletion in the space-charge layer at equilibrium.[49] The same dopant content is used in both materials, thus the $V_O^{\bullet\bullet}$ depletion is not likely to be more severe in BICUVOX0.10. Moreover, any significant variation of the sign of the space-charge potential may not be anticipated without any other solutes segregation.[54] No proofs of significant modification of the chemical composition at grain boundary interfaces were evidenced in the investigated samples to interpret the recorded blocking contributions. Therefore, no enhancement layer is likely to occur in BICOVOX0.10 to analyse the lower blocking effect. As suggested by Tuller,[55] the contribution of any space-charge conductivity to the main bulk one is expected to be far less significant in micrometer-sized grains. Accordingly, a space-charge effect was not regarded as dominating. Since BIMEVOX ceramics exhibit conduction anisotropy, one should expect that the electrical properties are dependent on grain size and also on grain morphology. In yttria-stabilised zirconia, a well-known isotropic ionic conductor, the blocking factor related to regular grain boundaries is a decreasing function of the average grain size.[33] Despite slightly larger grain dimensions, α_{gb} is higher in BICUVOX0.10.

For a given microstructure, the magnitude of the blocking effect is expected to depend only on the bulk conductivity of the material.[43] For instance the value of the blocking factor of BICOVOX0.10 is 0.10 when σ_b is equal to 3.2×10^{-5} S cm^{-1}. For the same specific conductivity, α_{gb}, recorded in high purity yttria-stabilised zirconia, whose grain morphology is nearly identical, was found to be 0.12[38] whereas it is equal to 0.38 in case of BICUVOX0.10. A detailed examination of SEM micrographs of both BIMEVOX0.10 materials (Fig. 6) shows that more plate-like grains are observed in dense BICUVOX0.10 ceramic. On the other hand, the depression angle, β_{gb}, of the blocking effect is slightly higher for this sample, whatever the oxygen partial pressure (Fig. 12). All these results suggest that the larger blocking contribution in BICUVOX0.10 can be interpreted in terms of a higher conduction anisotropy of regular grain boundaries because of an anisotropic grain growth. Another argument in favour of this assumption is that the grain boundary resistance of polycrystalline β-alumina ceramics was not found proportional to the average grain dimension when large grain aspect ratio were determined.[45] Accordingly, any comparison of the blocking effect in BIMEVOX0.10 materials should be meaningless because of too different sintering conditions.

3.4. Influence of the oxygen partial pressure

For a few ppm content, the activation energies determined from the Arrhenius diagram of the different conductivities (Fig. 9a and b) are not greatly altered (Table 3). Nevertheless, a slight increase in $E_{a,gb}$ was recorded for BICOVOX0.10 which results in a higher grain boundary conductivity in the low temperature region. For both materials, the electrolyte conductivity is only slightly reduced at low oxygen partial pressure. Even in this atmosphere, a curvature delimiting two temperature domains is evidenced on the Arrhenius diagram for BICUVOX0.10. Such a knee point was not observed for the Co-doped material (Fig. 9b), suggesting a slightly different conduction process, mostly above 450°C (as discussed below). According to the Arrhenius diagram of the relaxation frequencies, the apex frequency of the blocking effect was not strongly modified (Fig. 10). On the other hand, the bulk relaxation frequency greatly decreases within the whole measuring

temperature for both materials. This is related to large values of dielectric constant at 25°C: it is equal to 97 and 72 for Co- and Cu- doped materials respectively (Fig. 11). Regarding the grain boundary capacitance, the oxygen partial pressure has no real influence. The microstructure defects are therefore not modified in terms of geometrical parameters by varying the oxygen pressure. No change in the depression angle related to each semicircle was recorded (Fig. 12). Moreover, the blocking behaviour of both materials remains nearly identical (Fig. 13). At this stage, one can easily assume that varying the oxygen partial pressure in the intermediate temperature range does not significantly alter the electrical properties of both BIMEVOX0.10 materials.

3.5. Electrolytic domain, types of electronic conductivity and transport number

The accurate estimation of any electronic transport number in the investigated materials was performed by means of impedance spectroscopy. To neglect any interference of the blocking effect on the influence of oxygen partial pressure, impedance measurements were carried out above 450°C (Fig. 9a and b). Moreover, the upper limit was fixed at 650°C to prevent any eventual microstructure modification (which could alter the magnitude of the blocking effect) due to a partial sintering above this temperature (Fig. 5). Between 10^{-7} and 0.21 bar, no significant variation of the bulk conductivity was recorded for BICUVOX0.10 (Fig. 14). This is in concordance with the results of Fouletier et al.[17] on BICUVOX0.24 single crystal material in this temperature range, but in contradiction to the study of Iharada et al.[56] These authors estimated the electronic transport number of polycrystalline BICUVOX0.10 to be in the order of a few percent at 560°C by using Faraday measurements which did not reveal sufficiently accurate. In addition, the results could be spoilt due to cathodic reduction of BIMEVOX0.10 compounds. Moreover, the sintering conditions were not optimised and the recorded variations of the electrolyte conductivity are likely to be spoilt because of the time evolution. The global conductivity of the sample is the sum of the ionic and electronic conductivities, both being discriminated from each other by their related oxygen partial pressure dependence. The ionic conductivity do not depend on the oxygen partial pressure as the oxygen vacancy concentration is fixed by the BIMEVOX0.10 composition (electrolytic domain). The electronic conductivity is however strongly dependent on the oxygen partial pressure and the variations obey to the usual power laws. It is therefore possible to determine the electronic transport number of BIMEVOX0.10 compounds by following the variations of conductivity versus temperature and oxygen partial pressure. However, this method can be used for an electronic transport number greater than one percent, provided that the oxygen partial pressure variation is sufficiently wide. According to Fig. 14, BICUVOX0.10 material can be considered as a solid electrolyte with an ionic conductivity equal to 0.06, 0.12 and 0.2 S cm^{-1} at 450, 550 and 650°C, respectively, in the investigated $p(O_2)$ range and an electronic transport number lower than one percent. On the other hand, BICOVOX0.10 material seems to exhibit a small p-type conductivity for temperatures higher than 550°C and above 0.021 bar (Fig. 14). Such behaviour was already observed with BICOVOX0.20 for $p(O_2)$ higher than 10^{-4} bar above 530°C.[17] The higher the temperature, the larger the electronic contribution but the observed variations are too small to obey classical power laws. However, an electronic transport number of 3% was calculated with BICOVOX0.10 material at 650°C. If one refers to the Arrhenius diagram of the electrolyte conductivity (Fig. 9b) the electronic conduction process seems to play a significant role.

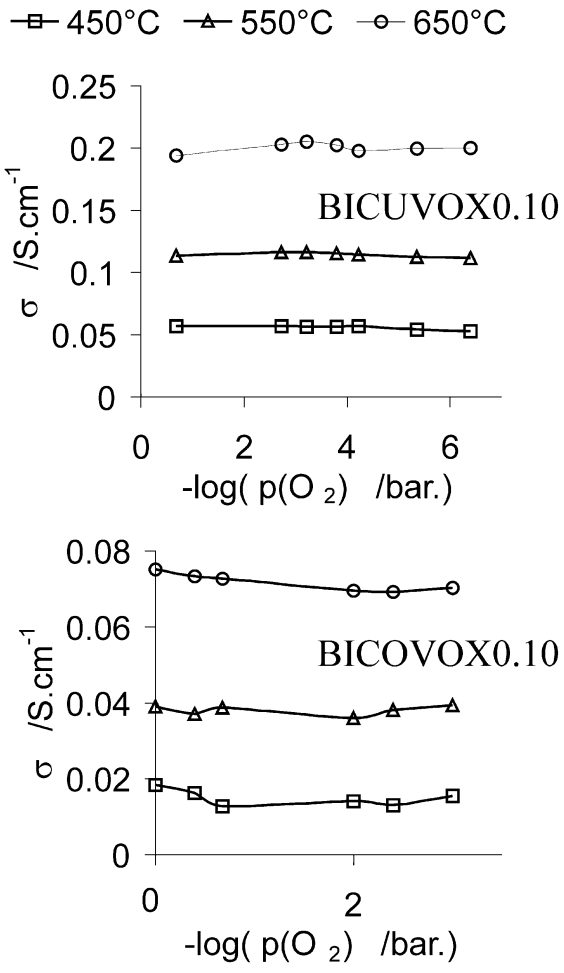

Fig. 14. Temperature- and $p(O_2)$-dependence of total electrical conductivity of both BICUVOX0.10 and BICOVOX0.10 measured at 450, 550 and 650°C in the 10^{-7}–1 bar $p(O_2)$ range.

4. Conclusions

The thermal history and the resultant local ordering of oxygen vacancies in BIMEVOX0.10 compounds could be inhibited by using a fine and homogeneous microstructure depending on starting reactive powder and sintering conditions as previously shown by Steil et al.[24] on BICOVOX0.10 compounds. Thus, no time-dependence and no hysteresis cycles of the total electrical conductivity were observed during subsequent thermal cycles. Electrical conductivity of BICUVOX0.10 material is 2 to 3 times higher than that of BICOVOX0.10 compound within the investigated experimental conditions. The nature of the dopant (Me = Cu or Co) revealed a great scatter in the electrical property which is characterised by a higher blocking effect with BICUVOX0.10 despite higher intragranular property. A small p-type electronic contribution to the bulk conductivity was noticed for BICOVOX0.10 material with a typical electronic transport number of 3% at 650°C in air atmosphere which precludes the use of the BICOVOX0.10 material in the oxygen electrochemical sensor. BICUVOX0.10 could be considered as mainly solid electrolyte in the 10^{-7}–1 bar oxygen partial pressure range for temperatures lower than 650°C. This last feature confers to the BICUVOX0.10 material a potential use in potentiometric or amperometric oxygen sensors. Moreover applications such as the electrochemical pumping of oxygen can take advantage of the high oxide ion conductivity at intermediate temperature.

Acknowledgements

This present study is part of a Research Program Contract (C.P.R., C.N.R.S.) involving five laboratories and an industrial research group, L'Air Liquide. The authors would like to thank the representatives of the CPR, G. Mairesse (LCPS-ENSCL, Lille) and P. Del Gallo (CRCD-Air Liquide, Paris).

References

1. Boivin, J. C. and Mairesse, G., Recent material developments in fast oxide ion conductors. *Chem. Mater.*, 1998, **10**, 2870–2888.
2. Subbarao, E. C., Zirconia — an overview. In *Advances in Ceramics, Vol. 3*, ed. A. H. Heuer and L. W. Hobbs. Am. Ceram. Soc, Columus, OH, USA, 1981, pp. 1–24.
3. Takahashi, T. and Iwara, H., High oxide ion conduction in sintered oxides of the system bismuth oxide-tungsten oxide. *J. Appl. Electrochem.*, 1973, **3**, 65–72.
4. Harwig, H. A. and Gerards, A. G., Electrical properties of α, β, γ and δ phases of bismuth sesquioxide. *J. Solid State Chem.*, 1978, **26**, 265–274.
5. Ishihara, T., Matsuda, H. and Takita, Y., Doped $LaGaO_3$ perovskite type oxide as a new oxide ionic conductor. *J. Am. Chem. Soc.*, 1994, **116**, 3801–3803.
6. Feng, M. and Goodenough, J. B., A superior oxide-ion electrolyte. *Eur. J. Solid State Inorg. Chem.*, 1994, **31**, 663–672.
7. Abraham, F., Debreuille-Gresse, M. F., Mairesse, G. and Nowogrocki, G., Phase transition and ionic conductivity in bismuth vanadate ($Bi_4V_2O_{11}$), an oxide with a layered structure. *Solid State Ionics*, 1988, **28-30**, 529–532.
8. Abraham, F., Boivin, J. C., Mairesse, G. and Nowogrocki, G., The BIMEVOX series: a new family of high performance oxide ion conductors. *Solid State Ionics*, 1990, **40-41**, 934–937.
9. Tuller, H. L., Semiconduction and mixed ionic-electronic conduction in nonstoichiometric oxides: impact and control. *Solid State Ionics*, 1997, **94**, 63–74.
10. Goodenough, J. B., Manthiram, A., Paranthaman, M. and Zhen, Y. S., Oxide ion conductors. *Mat. Sci. Eng.*, 1992, **B12**, 357–364.
11. Lazure, S., Vernochet, C., Vannier, R. N., Nowogrocki, G. and Mairesse, G., Composition dependence of oxide anion conduction in the BIMEVOX family. *Solid State Ionics*, 1996, **90**, 117–123.
12. Kurek, P. and Breiter, M. W., Thermal stability and ionic conductivity of the BIMEVOX0.10 ceramics (ME = Zn, Ni). *Solid State Ionics*, 1996, **86–88**, 131–135.
13. Dygas, J. R., Kurek, P. and Breiter, M. W., Structure-dependent impedance of BICUVOX. *Electrochim. Acta*, 1995, **40**, 1545–1550.
14. Vannier, R. N., Mairesse, G., Abraham, F., Nowogrocki, G., Pernot, E., Anne, M., Bacmann, M., Strobel, P. and Fouletier, J., Thermal behaviour of $Bi_4V_2O_{11}$: X-ray diffraction and impedance spectroscopy studies. *Solid State Ionics*, 1995, **78**, 183–189.
15. Pernot, E., Anne, M., Bacmann, M., Strobel, P., Fouletier, J., Vannier, R. N., Mairesse, G., Abraham, F. and Nowogrocki, G., Structure and conductivity of Cu and Ni-substituted $Bi_4V_2O_{11}$ compounds. *Solid State Ionics*, 1994, **70-71**, 259–263.
16. Kim, S. K. and Miyayama, M., Anisotropy in oxide ion conductivity of $Bi_4V_{2-x}Co_xO_{11-\delta}$. *Solid State Ionics*, 1997, **104**, 295–302.
17. Fouletier, J., Muller, C. and Pernot, E., Electrical anisotropy and electronic conductivity of BIMEVOX electrolytes. In *Electroceramics V*, ed. J. L. Baptista, J. A. Labrincha and P. M. Vilarinho. University of Aveiro, Portugal, 1996, pp. 37–46.
18. Krok, F., Abrahams, I., Bangobango, D. G., Bogusz, W. and Nelstrop, J. A. G., Electrical and structural study of BICOVOX. *Solid State Ionics*, 1996, **86–88**, 261–266.
19. Krok, F., Abrahams, I., Bangobango, D. G., Bogusz, W. and Nelstrop, J. A. G., Structural and electrical characterisation of BINIVOX. *Solid State Ionics*, 1998, **111**, 37–43.
20. Lee, C. K. and West, A. R., Thermal behaviour and polymorphism of BIMEVOX oxide ion conductors including the new materials: $Bi_4V_2O_{11}$: M; M = La, Y, Mg, B. *Solid State Ionics*, 1996, **86–88**, 235–239.
21. Simner, S. P., Suarez-Sandoval, D., Mackenzie, J. D. and Dunn, B., Synthesis, densification, and conductivity characteristics of BICUVOX oxygen-ion-conducting ceramics. *J. Am. Ceram. Soc.*, 1997, **80**, 2563–2568.
22. Reiselhuber, K., Dorner, G. and Breiter, M. W., Studies of BICUVOX0.10 by conductivity measurements and differential thermal analysis. *Electrochim. Acta*, 1993, **38**, 969–973.
23. Dygas, J. R., Krok, F., Bogusz, W., Kurek, P., Reiselhuber, K. and Breiter, M. W., Impedance study of BICUVOX ceramics. *Solid State Ionics*, 1994, **70-71**, 239–247.
24. Steil, M. C., Fouletier, J., Kleitz, M. and Labrune, P., BICOVOX: sintering and grain size dependence of the electrical properties. *J. Eur. Ceram. Soc.*, 1999, **19**, 815–818.
25. Bauerle, J. E., Study of solid electrolyte polarisation by a complex admittance method. *J. Phys. Chem. Solids*, 1969, **30**, 2657–2660.
26. Bonanos, N., Steele, B. C. H., Butler, E. P., Johnson, W. B., Worell, W. L., Macdonald, D. D. and McKubre, M. C. H., Applications of Impedance Spectroscopy. In *Impedance Spectroscopy*, ed. J. R. Macdonald. John Wiley and Sons, New York, USA, 1987, pp. 191–340.

27. Gür, T. M., Raistrick, I. D. and Huggins, R. A., AC admittance measurements on stabilised zirconia with porous platinum electrodes. *Solid State Ionics*, 1980, **1**, 251–271.
28. Van Hassel, B. A., Boukamp, B. A. and Burggraaf, A. J., Electrode polarisation at the Au, O_2 (g)/Fe implanted yttria-stabilised zirconia interface. *Solid State Ionics*, 1992, **51**, 161–174.
29. Schouler, E. J., Etude des Cellules à Oxyde Electrolyte Solide par la Méthode des Impédances Complexes. Thesis, Institut National Polytechnique de Grenoble, 1979.
30. Mendelson, M. I., Average grain size in polycrystalline ceramics. *J. Am. Ceram. Soc.*, 1969, **52**, 443–446.
31. Urquidi-Macdonald, M., Real, S. and Macdonald, D. D., Applications of Kramers–Kronig transforms in the analysis of electrochemical impedance data. III Stability and linearity. *Electrochim. Acta*, 1990, **35**, 1559–1566.
32. Spinolo, G., Chiodelli, G., Magistris, A. and Tamburini, U. A., Data processing for electrochemical measurements with frequency response analysers. *J. Electrochem. Soc.*, 1988, **135**, 1419–1424.
33. Bernard, H., *Microstructure et Conductivité de la Zircone Frittée*. Thesis, Institut National Polytechnique de Grenoble, 1980.
34. Dessemond, L., *Spectroscopie d'Impédance des Fissures dans la Zircone Cubique*. Thesis, Institut National Polytechnique de Grenoble, 1992.
35. Fleig, J. and Maier, J., The impedance of ceramics with highly resistive grain boundaries: validity and limits of the brick layer model. *J. Eur. Ceram. Soc.*, 1999, **19**, 693–696.
36. Fleig, J. and Maier, J., A finite element study on the grain boundary impedance of different microstructures. *J. Electrochem. Soc.*, 1998, **145**, 2081–2089.
37. Van-Dijk, T. and Burggraaf, A. J., Grain boundary effects on ionic conductivity in ceramic $Gd_xZr_{1-x}O_{2-x/2}$ solid solutions. *Phys. Stat. Sol. (A)*, 1981, **63**, 229–240.
38. Steil, M. C., Thevenot, F. and Kleitz, M., Densification of yttria-stabilised zirconia: Impedance spectroscopy analysis. *J. Electrochem. Soc.*, 1997, **144**, 390–398.
39. Fleig, J., The influence of non-ideal microstructure on the analysis of grain boundary impedances. *Solid State Ionics*, 2000, **131**, 117–127.
40. Krok, F., Bogusz, W., Kurek, P., Wasiucionek, M., Jakubowski, W. and Dygas, J. R., Influence of preparation procedure on some physical properties of BICUVOX. *Mater. Sci. Eng.*, 1993, **B21**, 70–76.
41. Joubert, O., Jouanneaux, A., Ganne, M., Vannier, R. N. and Mairesse, G., Solid phase synthesis and characterisation of new BIMEVOX series: $Bi_4V_{2-x}M_xO_{11-x}$ ($M = Cr^{III}$, Fe^{III}). *Solid State Ionics*, 1996, **83**, 199–207.
42. Dessemond, L., Mucillo, R., Henault, M. and Kleitz, M., Electric conduction-blocking effects of voids and second phases in stabilised zirconia. *Appl. Phys. A*, 1993, **57**, 57–60.
43. Kleitz, M., Dessemond, L. and Steil, M. C., Model for ion-blocking at internal interfaces in zirconias. *Solid State Ionics*, 1995, **75**, 107–115.
44. Ovenston, A., Effect of atmosphere on the electrical properties of polycrystalline yttria-stabilised zirconia. *Solid State Ionics*, 1992, **58**, 221–229.
45. Funke, K., Ion transport in fast ion conductors — spectra and models. *Solid State Ionics*, 1997, **94**, 27–33.
46. De-Jonghe, L. C., Grain boundaries and ionic conduction in sodium beta alumina. *J. Mater. Sci.*, 1979, **14**, 33–48.
47. Lee, C. K., Sinclair, D. C. and West, A. R., Stoichiometry and stability of bismuth vanadate, $Bi_4V_2O_{11}$, solid solutions. *Solid State Ionics*, 1993, **62**, 193–198.
48. Ciacchi, F. T., Crane, K. M. and Badwal, S. P. S., Evaluation of commercial zirconia powders for solid oxide fuel cells. *Solid State Ionics*, 1994, **73**, 49–61.
49. Guo, X., Physical origin of the intrinsic grain-boundary resistivity of stabilised-zirconia: role of the space-charge layers. *Solid State Ionics*, 1995, **81**, 235–242.
50. Frenkel, J., *Kinetic Theory of Liquids*. Oxford University Press, New York, USA, 1946.
51. Lehovec, K., Space charge layer and distribution of lattice defects at the surface of ionic crystals. *J. Chem. Phys.*, 1953, **21**, 1123–1128.
52. Kliewer, K. L. and Koelher, J. S., Space charge in ionic crystal I, general approach with application to NaCl. *Phys. Rev. A*, 1965, **140**, 1126–1140.
53. Eshelby, J. D., Newey, C. W. A., Pratt, P. L. and Lidiard, A. B., Charged dislocations and the strength of ionic crystals. *Phil. Mag.*, 1958, **3**, 75–89.
54. Guo, X., Solute segregations at the space-charge layers of stabilized zirconia: an opportunity for ameliorating conductivity. *J. Eur. Ceram. Soc.*, 1996, **16**, 575–578.
55. Tuller, H. L., Ionic conduction in nanocrystalline materials. *Solid State Ionics*, 2000, **131**, 143–157.
56. Iharada, T., Hammouche, A., Fouletier, J., Kleitz, M., Boivin, J. C. and Mairesse, G., Electrochemical characterisation of BIMEVOX oxide-ion conductors. *Solid State Ionics*, 1991, **48**, 257–265.